Title: Transient Polycomb activity represses developmental genes in growing oocytes.

Authors: Ellen G. Jarred[1], Zhipeng Qu[2], Tesha Tsai[1], Ruby Oberin[1], Sigrid Petautschnig[1], Heidi Bildsoe[1], Stephen Pederson[2], Qing-hua Zhang[3], Jessica M. Stringer[3], John Carroll[3], David K. Gardner[4], Maarten van den Buuse[5], Natalie A. Sims[6], William T. Gibson[7], David L. Adelson[2], Patrick S. Western[1]*

Affiliations: [1]Centre for Reproductive Health, Hudson Institute of Medical Research and Department of Molecular and Translational Science, Monash University, Clayton, Victoria, Australia; [2]Department of Bioinformatics and Computational Genetics, School of Biological Sciences, University of Adelaide, Adelaide, South Australia, Australia; [3]Biomedicine Discovery Institute, Monash University, Clayton, Victoria, Australia; [4]School of BioSciences, University of Melbourne, Parkville, Victoria, Australia; [5]School of Psychology and Public Health, La Trobe University, Melbourne, Victoria, Australia; [6]Bone Cell Biology and Disease Unit, St. Vincent's Institute of Medical Research and Department of Medicine at St. Vincent's Hospital, Fitzroy, Victoria, Australia; [7]Department of Medical Genetics, University of British Columbia and British Columbia Children's Hospital Research Institute, Vancouver, BC, Canada.

* Corresponding author: patrick.western@hudson.org.au

Abstract

Background: Non-genetic disease inheritance and offspring phenotype is substantially influenced by germline epigenetic programming, including genomic imprinting. Loss of Polycomb Repressive Complex 2 (PRC2) function in oocytes causes non-genetically inherited effects on offspring, including embryonic growth restriction followed by post-natal offspring overgrowth. While PRC2 dependent non-canonical imprinting is likely to contribute, less is known about germline epigenetic programming of non-imprinted genes during oocyte growth. In addition, *de novo* germline mutations in genes encoding PRC2 lead to overgrowth syndromes in human patients, but the extent to which PRC2 activity is conserved in human oocytes is poorly understood.

Results: In this study we identify a discrete period of early oocyte growth during which PRC2 is expressed in mouse growing oocytes. Deletion of *Eed* during this window led to the de-repression of 343 genes. A high proportion of these were developmental regulators, and the vast majority were not imprinted genes. Many of the de-repressed genes were also marked by the PRC2-dependent epigenetic modification histone 3 lysine 27 trimethylation (H3K27me3) in primary-secondary mouse oocytes, at a time concurrent with PRC2 expression. In addition, we found H3K27me3 was also enriched on many of these genes by the germinal vesicle (GV) stage in human oocytes, strongly indicating that this PRC2 function is conserved in the human germline. However, while the 343 genes were de-repressed in mouse oocytes lacking EED, they were not de-repressed in pre-implantation embryos and lost H3K27me3 during pre-implantation development. This implies that H3K27me3 is a transient feature that represses a wide range of genes in oocytes.

Conclusions: Together, these data indicate that EED has spatially and temporally distinct functions in the female germline to repress a wide range of developmentally important genes, and that this activity is conserved in the mouse and human germlines.

Keywords

Polycomb, oocyte, programming, epigenetic, H3K27me3, inheritance

Background

Epigenetic modifications, including DNA methylation and histone modifications, regulate chromatin packaging and underlie long-term cell-specific gene transcription patterns. Amongst other chromatin regulatory functions, many of these modifications are essential for cell differentiation and provide mechanisms for maintaining lineage-specific identity and cell functions through the life of an organism. Conversely, dysregulation of epigenetic modifications contributes to a wide range of diseases and syndromes, including congenital anomalies, cancer, diabetes and behavioural conditions (1-4).

The maternal and paternal genomes transmit genetic and epigenetic information to offspring at fertilisation. While oocyte and sperm chromatin are respectively organised in distinct histone and protamine-mediated structures, the vast majority of maternal and paternal alleles achieve epigenetic equivalence within a short period after fertilisation, a process that relies partly on proteins and RNAs that are maternally inherited in the oocyte. However, some genes maintain parent-specific epigenetic patterns that were established during sperm and oocyte development. In mice and humans, these genes include around 120 imprinted genes that are typically marked either by maternal or paternal DNA methylation, an epigenetic state that is transmitted to, and maintained in offspring and is essential for parent-of-origin specific gene regulation during development (5-8). While genomic imprinting provides an unequivocal example of epigenetic inheritance, evidence for other epigenetically inherited states that may affect biallelically expressed genes are rare and the mechanisms underlying such inheritance are poorly understood (5). Given the potential for epigenetic states to influence offspring development, identifying the specific chromatin-modifying complexes that epigenetically regulate developmental genes and may influence establishment of an appropriate epigenetic landscape in oocytes would enhance understanding of the mechanisms underlying inherited phenotypes and disease, and of how these mechanisms may contribute to evolution.

Histone 3 Lysine 27 trimethylation (H3K27me3) is a critical epigenetic modification catalysed by the Polycomb Repressive Complex 2 (PRC2). PRC2 contains three essential core protein subunits: Suppressor of Zeste 12 (SUZ12), Embryonic Ectoderm Development (EED) and Enhancer of Zeste 1/2 (EZH1/2), all of which are required for histone methyltransferase activity (9-12). While EZH2

can function in PRC2-independent roles, EED is only known to mediate methylation of H3K27 as an essential component of PRC2 (13-19). Specific examples include an essential role for EED in repressing a wide range of developmentally important genes in embryonic stem cells (ESCs) through its essential role in establishing H3K27me3 (12, 20). While EZH2 also plays a major role in the repression of the same genes, the closely related protein EZH1 acts in a partially redundant manner and contributes both to H3K27me3 enrichment and gene repression (12). In other contexts, EZH2 can directly methylate non-histone target proteins such as PLZF in B lymphocytes of the immune system, and GATA4 in mouse fetal cardiomyocytes *in vivo* (13, 17).

PRC2 also plays important roles in sperm and oocytes, and throughout development. *De novo* germline mutations in human *EED, EZH2* and *SUZ12* underlie Cohen-Gibson, Weaver and Imagawa-Matsumoto syndromes which are characterised by perinatal overgrowth, skeletal malformation and cognitive deficit (21-30). Multiple studies in mice indicate that EZH2 and EED act as maternal factor proteins and/or mRNA that are required in mature oocytes to regulate the establishment and maintenance of X-inactivation in pre-implantation embryos (31-34). In addition, PRC2 regulates DNA methylation-independent non-canonical imprinting in mouse oocytes, a process that involves H3K27me3-dependent programming and paternally-biased expression of up to 20 genes in pre-implantation embryos and five genes in extraembryonic ectoderm and placenta until embryonic day (E)9.5 (8, 35). Maternal deletion of *Eed* resulted in loss of H3K27me3 imprints, biallelic expression of H3K27me3-imprinted genes in pre-implantation embryos and extraembryonic ectoderm, transient ectopic X-inactivation and male-biased embryo loss (33, 34). Moreover, mouse offspring generated by somatic cell nuclear transfer (SCNT) are typically born large as a result of placental hyperplasia, a phenotype that is caused by loss of H3K27me3 imprinting primarily of *Slc38a4* and *Sfmbt2*-embedded micro-RNAs specifically in the placenta (36-38). Although H3K27me3 imprinting specifically affects the placenta, embryonic growth restriction was also observed in embryos derived from oocytes lacking EED, but the cause of this phenotype is not understood (33). While H3K27me3-dependent imprinting (non-canonical) has been recently identified, classical (or canonical) genomic imprinting is much more extensively studied and is generally considered to be mediated by DNA methylation (8, 39). Here, we refer to canonical DNA methylation-based genomic imprints as classical imprinting and non-canonical imprinting as H3K27me3-dependent imprinting.

We previously found that deletion of *Eed* in growing oocytes led to post-natal overgrowth of offspring, indicating that maternally-derived PRC2 mediates effects on offspring that were independent of maternal genetic inheritance (40). To understand the potential mechanisms underlying developmental outcomes in offspring from *Eed* null oocytes, we explored the role of PRC2 in oocytes. We demonstrate that EZH2, EED and SUZ12 are transiently expressed during the earliest stages of oocyte growth to establish H3K27me3 in the promoters of developmentally important genes in mice, and that H3K27me3 is conserved on many of these genes in human GV stage oocytes. In mice, PRC2 activity immediately preceded the upregulation of the essential *de novo* DNA methylation co-factor DNMT3L, indicating that patterning of PRC2 target genes precedes DNA methylation. While *Eed* repressed several imprinted genes in oocytes, 98% of the PRC2 target genes we identified were not imprinted, but were genes that regulate neurogenesis, haematopoiesis and other processes in tissue morphogenesis. These genes were not dysregulated in pre-implantation offspring and lost H3K27me3 during this period of development in wild type (*wt*) embryos.

Results

EZH2, EED and SUZ12 localise to chromatin during a discrete period of primary to secondary oocyte growth

Previous studies have provided varying reports of EED, EZH2 and SUZ12 in GV stage and mature oocytes, and zygotes (31, 41-43), but the stages at which all three core components of PRC2 are detected in growing oocytes have not been defined. To determine when PRC2 is detected in the nucleus or associated with chromosomes in growing, GV and MII oocytes, and in zygotes, we profiled EZH2, SUZ12 and EED throughout oocyte growth in *wt* mice using immunofluorescence (IF). EZH2 was detected in the oocyte nucleus of primordial to antral stage follicles, but SUZ12 and EED were detected only in primary and secondary follicle oocytes and not in primordial or antral stage oocytes (Fig. 1A). Notably, co-expression of EED, EZH2 and SUZ12 in primary-secondary follicle oocytes occurred immediately before the expression of DNMT3L (DNA methyltransferase 3-Like), which marks the onset of *de novo* DNA methylation in growing oocytes (Fig. 1B), consistent with the initiation of H3K27me3 in oocytes prior to DNA methylation (44). While EZH2 was detected in the nuclei of fully-grown surrounded nucleolus (SN) GV oocytes, SUZ12 and EED were not (Fig. 1C). Although PRC2 has been detected in the cytoplasm of mature metaphase II (MII) oocytes (41-43), EED, EZH2 and SUZ12 were not detected on the chromosomes

of MII oocytes in this study (Fig. 1D). However, all three PRC2 components were readily detected in maternal and paternal pronuclei of zygotes approximately 12 hours (h) post-fertilization (Fig. 1E). As embryonic activity of PRC2 does not occur until the 4-cell to morula stage (31, 34), the rapid recruitment of PRC2 to the pronuclei may reflect a supply of cytoplasmic PRC2 proteins (41-43) or could be derived from mRNAs in the mature oocyte. Taken together, these data identify a transient window during which all three PRC2 components are present and may therefore contribute to PRC2-dependent epigenetic programming in primary-secondary oocytes, immediately before genome-wide *de novo* DNA methylation and prior to the formation of GV-oocytes.

PRC2 is required for repression of developmental genes in growing oocytes

To investigate whether the transient activity of PRC2 in oocytes of primary-secondary follicles has functional importance, we deleted *Eed* using *Zp3Cre*, which leads to target gene excision specifically in oocytes from the primary follicle stage (40, 45). Mating $Eed^{fl/fl}$ females and $Eed^{fl/+}$*;Zp3Cre* males yielded $Eed^{fl/fl}$ (*Eed-wt*), $Eed^{fl/+}$*;Zp3Cre* (*Eed-het*) and $Eed^{fl/fl}$*;Zp3Cre* (*Eed-hom*) females. Following deletion of *Eed*, H3K27me3 was reduced by 35% in primary follicles of *Eed-hom* females (Fig. 2A-B). Depletion of H3K27me3 continued in secondary follicles (Fig. 2A, C), and was almost completely lost in fully-grown GV oocytes, with 85% and 93% reductions in global H3K27me3 in *Eed-hom* oocytes compared to *Eed-wt* at these stages respectively (Fig. 2A, 2C, 3A-B).

To determine how loss of H3K27me3 impacted oocyte transcription, we collected *Eed-wt*, *Eed-het, Eed-hom* and $Eed^{+/+}$*;Zp3Cre* (*Eed-wt Cre* control) fully-grown SN GV oocytes and performed RNA-seq. The proportion of SN GV oocytes in *Eed-hom* females was 65% compared to 58% in *Eed-wt* females (Supp. Fig. 1), demonstrating that loss of EED and H3K27me3 did not detrimentally affect formation of fully-grown oocytes. Principal component analysis revealed that *Eed-hom* oocytes were transcriptionally distinct from *Eed-het* and *Eed-wt* oocytes (Fig. 3C). Further analysis identified 349 genes that we termed *Eed* oocyte Differentially-Expressed Genes (DEGs) as they were differentially expressed between *Eed-hom* and *Eed-het* oocytes (FDR<0.05; Fig. 3D; Supp. Table 1). Strikingly, 98% (343 genes) of the *Eed* oocyte DEGs were derepressed, and only 2% (six genes), including *Eed,* were downregulated (Fig. 3D-E; Supp. Table 1). H3K27me3 levels were not different and only two *Eed* oocyte DEGs (*Mt1* and *Exoc)* as well as *Eed* were identified between

179 *Eed-wt* and *Eed-het* oocytes (Fig. 3A-B), indicating that EED function in *Eed-wt* and *Eed-het*
180 oocytes was similar. As EED protein was only detected in primary-secondary oocytes prior to the
181 GV stage, these data strongly indicate that PRC2 establishes a repressive state in primary and
182 secondary follicle oocytes that is maintained in GV oocytes.
183
184 Gene ontology (GO) and ingenuity pathway analyses (IPA) revealed that the *Eed* oocyte DEGs
185 were strongly associated with fetal development, including the IPA categories of nervous system
186 development (23.81%), haematopoiesis (23.81%), cell migration and morphology (21.43%) and
187 developmental disorders (19.05%; Fig. 3F-G). Several genes involved in bone development,
188 including *Prrx*, *Gli2*, *Sox5*, *Sox6*, *Hoxd9*, *Hoxd13*, *Bmp7*, *Sik3* and *Dcn* were also de-repressed
189 (Supp. Table 1). The neurogenesis and bone developmental genes are of interest as impaired
190 skeletal and cognitive development are prominent features of Cohen-Gibson syndrome which
191 results from *de novo* germline mutations in *EED* (21-23, 26). Although 4.67% of the *Eed* oocyte
192 DEGs were associated with "litter size and fertility", categories associated with oocyte or ovarian
193 development were not represented (Fig. 3G). Moreover, similar numbers of oocytes in *Eed-hom,*
194 *Eed-het* and *Eed-wt* females indicated that oocyte growth and formation of fully-grown oocytes
195 was not impeded (Supp. Fig. 1). Together, these observations strongly suggested that PRC2
196 establishes repressive H3K27me3 on a wide range of developmentally important genes during
197 oocyte growth, >95% of which were not primarily involved in oogenesis. Surprisingly, comparison
198 of the *Eed* oocyte DEGs with 209 transcription factors identified as direct target genes of PRC1
199 and PRC2 in embryonic stem cells (20) identified only 8 common genes (*Hoxd9, Hoxd13, Otx1,*
200 *Lhx2, Six1, Nr2f2, Ovol1* and *Nfatc1*), indicating that the genes that were de-repressed on *Eed* null
201 oocytes were not typical Polycomb target genes in ESCs (Supp Table 2).
202
203 **PRC2 regulates establishment of H3K27me3 on developmental genes in growing oocytes**
204 To determine whether H3K27me3 was normally present in the promoters of *Eed* oocyte DEGs in
205 GV oocytes we compared the *Eed* oocyte DEGs to H3K27me3 Chromatin Immunoprecipitation-
206 sequencing (ChIP-seq) datasets from wild type mouse GV and MII oocytes from Zheng and
207 colleagues and Liu and colleagues (44, 46). Of 349 *Eed* oocyte DEGs, the majority were identified
208 both in the Zheng and Liu datasets (328 in Zheng, and 312 in Liu). Of the 328 genes from Zheng *et*
209 *al.,* 111 (34%) and 127 (39%) had H3K27me3 peaks in GV and MII oocyte datasets, and 169 (52%)
210 had H3K27me3 peaks in the Liu MII dataset (Supp Table 3). Comparison of all datasets (our *Eed*

oocyte DEGs with the Zheng GV and MII and Liu MII datasets) identified 99 DEGs with H3K27me3 in all three ChIP-seq datasets, which we defined as 'high confidence H3K27me3-enriched oocyte DEGs (Fig. 4A; Supp. Table 4). Of these 99 genes, comparison with data from a study of H3K27me3 in sperm (47) revealed that 88 also carried H3K27me3 on the paternal allele indicating that the majority of these genes are subject to H3K27 methylation in both the male and female germlines (Supp. Table 4). While only ~30% of the *Eed* oocyte DEGs contained H3K27me3 under these highly stringent criteria, we propose that this is a conservative estimate given that low input ChIP-seq data were used, potentially limiting sensitivity compared to RNA-seq analysis. Supporting this, 114 H3K27me3-enriched DEGs overlapped between the Liu and Zheng MII datasets, indicating that not all genes with H3K27me3 were consistently detected in the ChIP-seq analyses.

Gradual enrichment of H3K27me3 has been demonstrated in growing oocytes (44). Using these additional ChIP-seq datasets (44), we next investigated at what stage H3K27me3 peaks were established at the high confidence H3K27me3-enriched oocyte DEGs by determining the H3K27me3 state at the promoter regions of these genes in post-natal day (P)7 (primary) and P14 (secondary) growing oocytes. None of the 99 high confidence H3K27me3-enriched oocyte DEGs had H3K27me3 peaks in primary (P7) oocytes, but 83 had H3K27me3 peaks in secondary (P14) oocytes and all 99 DEGs had H3K27me3 in GV and MII oocytes (Fig. 4B; Supp. Table 4). Accordingly, each of these genes were upregulated in *Eed-hom* GV oocytes (Fig. 4C). Collectively, these data demonstrate that H3K27me3 was established within the promoters of developmental genes during the window in which all three core components of PRC2 were detected in primary-secondary oocytes and that EED was required for their repression given that these genes were de-repressed in *Eed*-null GV oocytes.

PRC2 establishment of H3K27me3 at developmental genes is conserved in human oocytes

To understand whether the mouse *Eed* oocyte DEGs were also enriched for H3K27me3 in human oocytes, we examined published H3K27me3 data from human GV oocytes (48), defining promoter regions 2000bp upstream – 2000bp downstream of the TSS as we did for the mouse datasets. Of 349 *Eed* oocyte DEGs, 37 were excluded as 'not conserved in human', including 25 predicted genes, RIKEN transcripts or pseudogenes (Fig. 4D; Supp. Table 3). Of the 312 remaining *Eed* oocyte DEGs, 132 contained H3K27me3 in their promoters in human GV oocytes (Fig 4D; Supp. Table 3; Supp. Table 5). Of the 132 *Eed* oocyte DEGs containing H3K27me3 in human GV oocytes, 79 and

54 also contained H3K27me3 in the mouse MII and GV datasets generated by Liu *et al.* and Zheng *et al.*, respectively (Supp. Table 5 (44, 46)). Moreover, all 132 *Eed* oocyte DEGs identified as H3K27me3 enriched in human were upregulated in *Eed-hom* oocytes (Fig. 4E). In common with the lack of nuclear-localised EED or SUZ12 protein in mouse GV oocytes (Fig. 1C), human GV oocytes lack *EED* and *SUZ12* transcripts (48). Together, with the observation that *Eed* oocyte DEGS are almost exclusively de-repressed with the loss of EED and H3K27me3, these data strongly indicate that H3K27me3 establishment occurs on *Eed* oocyte DEGs prior to the GV stage in both human and mouse growing oocytes.

Eed oocyte DEGs include non-imprinted autosomal, imprinted and X-linked genes

As EED regulates DNA methylation-independent H3K27me3 imprinting in oocytes, we compared the *Eed* oocyte DEGs against a previously published list of 76 putative H3K27me3-imprinted genes (35). Of the 349 *Eed* oocyte DEGs we identified in GV oocytes, five (*Bbx, Bmp7, Rbms1, Sall3* and *Prox1*) were putative H3K27me3 imprinted genes (Fig. 5A; Supp. Table 6). These genes were all upregulated in *Eed-hom* oocytes (Fig. 5B), demonstrating that EED is required for their repression in oocytes. Of interest, analysis of a sperm ChIP-seq dataset (47) revealed that all five genes also contained H3K27me3 on the paternal allele, indicating that these genes have similar H3K27me3 signatures in male and female gametes (Supp. Table 3). Of these five genes, paternally biased expression was observed for three in androgenetic morula (*Bbx, Bmp7* and *Rbms1*) and one in blastocysts (*Rbms1*) (35). Notably, Inoue *et al*. identified five H3K27me3-imprinted genes (*Gab1, Phf17, Sfmbt2, Slc38a4 and Smoc1*) that maintain paternal biased expression in epiblast, visceral endoderm, extra-embryonic ectoderm and/or E9.5 placenta (35). Loss of imprinting at either *Slc38a4* or micro-RNAs within *Sfmbt2* has been functionally associated with placental hyperplasia in SCNT derived offspring (36, 38). In addition, *Smoc1* and *Gab1* have also been implicated in this phenotype (37). However, none of these genes were *Eed* oocyte DEGs (Supp. Table 6).

In order to determine whether any *Eed* oocyte DEGs were imprinted genes, we also compared the 349 *Eed* oocyte DEGs to 325 known or predicted classically imprinted genes in mice (49, 50). Ten *Eed* oocyte DEGs were identified as imprinted genes (Fig. 5C; Supp. Table 6; *Zdbf2, Ifitm10, Phlda2, Rbms1, Bmp7, Bbx, Flt3, Slc22a18, Cobl* and *Cysltr2*). As with the putative H3K27me3-imprinted genes, these were all upregulated in *Eed-hom* oocytes (Fig. 5D) indicating that EED is required to silence these genes in oocytes. Analysis of the sperm dataset (47) revealed that all of

these genes contained H3K27me3 on the paternal allele in sperm and three of these genes (*Bbx, Bmp7* and *Rbms1*) were also included on the H3K27me3-imprinted gene list (Supp. Table 3). In human GV oocytes *Bmp7, Sall3, Prox1, Zdbf2, Phlda2, Flt3* and *Ifitm10* also carried H3K27me3, but *Bbx, Rbms1, Cysltr2* and *Slc22a4* did not.

In mice, X-inactivation is initiated after fertilisation from the 2/4 cell stage and is restricted to the paternal X-chromosome in pre-implantation offspring prior to establishment of random X-inactivation in embryonic cells after implantation. While PRC2 regulates X-inactivation in pre-implantation embryos and somatic cells of post-implantation embryos, the inactive X is reactivated in XX primordial germ cells and both X-chromosomes are active in growing oocytes (51-53). To determine whether there was any bias in gene silencing across the autosomes and the X-chromosome in EED-deficient oocytes we determined the relative representation of the *Eed* oocyte DEGs across all chromosomes. However, representation of the oocyte DEGs across the autosomes and X-chromosome was similar, with 19 of 349 genes X-located and no substantial bias towards the X-chromosome or particular autosomes (Fig. 5E; Supp. Table 7). As with most genes on the autosomes, of the 19 X-linked genes identified, 18 were upregulated in *Eed-hom* oocytes (Fig. 5F) demonstrating that EED and H3K27me3 contribute to silencing individual X-linked genes in the absence of X inactivation in oocytes.

Together, these data indicated that of the 349 *Eed* oocyte DEGs identified, 12 were imprinted genes, 19 were located on the X-chromosome and the remaining 328 were non-imprinted autosomal genes, many of which are known to regulate development.

LINE-1 transposable elements were not de-repressed in *Eed*-null oocytes

Previous studies have proposed and/or demonstrated a link between H3K27me3 and the repression of transposable elements (TEs) in fetal germ cells and embryonic stem cells when DNA methylation levels are low during epigenetic reprogramming (54-57). To determine whether transcription of transposable elements was affected in oocytes lacking EED, we demasked repeat sequences in our RNA-seq data and analysed the expression of LINE-1 (L1) elements. The total input reads indicated that similar percentages of L1 element reads aligned in *Eed-hom*, *Eed-het* and *Eed-wt* oocytes (Supp. Fig. 2A). Moreover, regardless of whether elements mapped uniquely or multi-mapped, read totals indicated similar expression levels for L1s in oocytes of all genotypes

(Supp. Fig. 2B). Analysis of the extent to which multiple reads occurred revealed that the majority of reads mapped 1, 2 or 3 times (accounting for ~80% of all reads), while around 10% mapped 4-5 times and the remaining reads mapped 5-20 times, with no differences in mapping between genotypes (Supp. Fig. 2C). Principal component analysis revealed overlapping clusters for samples for all genotypes and no differentially expressed L1 elements were identified based on a threshold of FDR<0.05 (Fig. 6A, B). Together these data indicate that loss of H3K27me3 in GV oocytes did not substantially alter L1 expression.

Eed oocyte DEGs were not dysregulated in pre-implantation embryos

Our observations revealed a highly specific window during which all three components of PRC2 were present in primary-secondary oocytes and identified a role for EED in establishing H3K27me3 on a wide range of developmentally important genes in primary-secondary stage oocytes. As >95% of these genes are not known to regulate oocyte development, yet EED is required for their repression in oocytes, we proposed that loss of EED-dependent repression of these genes in oocytes may result in their de-repression in pre-implantation embryos. To determine if this was the case we re-analysed RNA-seq data from morula and blastocysts derived from *Gdf9Cre Eed* null (33) and *Zp3Cre Eed* null oocytes (34). The *Eed*-deleted oocyte-derived morulae contained 128 DEGs (P<0.05, all with FDR~1.0; Supp. Table 8) and the blastocysts contained 400 DEGs (P<0.05; FDR<0.05; Supp. Table 9) compared to their *Eed-wt* oocyte-derived counterparts. Six *Eed* oocyte DEGs were dysregulated in morulae (*Plxnd1, Tceal8, Rap2c, Bbx, Xlr3c* and *Trmt2b;* Supp. Fig. 3), and five were dysregulated in blastocysts (*Chrdl1, Lonrf2, Trim6, Cyp1b1* and *Ccbe1*; Supp. Fig. 3). With the exception of *Tceal8* and *Bbx*, all were downregulated in pre-implantation embryos derived from *Eed*-null oocytes (Supp. Tables 8-9). Only two genes were commonly downregulated in the morulae and blastocyst datasets (*Tspan6* and *Gk*) and no genes were dysregulated in all three datasets (Supp. Fig. 3). Similarly, there were no genes in the morula DEGs and only seven genes (*Zfpm2, Pax9, Tbx4, Foxc2, Atoh8, Msx1* and *Vsx1*) in the blastocyst DEGs that were common with 209 genes identified as direct Polycomb target transcription factors in ESCs (Supp. Table 10; (20)).

To determine whether H3K27me3 was maintained at *Eed* oocyte DEGs in pre-implantation embryos, we used CUT&RUN data revealing the H3K27me3 state on the maternal and paternal alleles in morula stage embryos (Supp. Table 3) (33). Six *Eed* oocyte DEGs contained H3K27me3

on the maternal, but not the paternal allele in morula. Of the remaining 343 *Eed* oocyte DEGs, 322 were devoid of H3K27me3 on both the maternal and paternal alleles. The maternal and paternal alleles were not distinguishable for 21 genes in the source dataset (33). These data indicate that H3K27me3 is normally cleared from the vast majority of *Eed* oocyte DEGs in morula stage embryos.

Discussion

In this study, we identified a discrete period during which all three core components of PRC2 co-localised to the nucleus in primary-secondary oocytes, that H3K27me3 was established on a wide range of developmental genes in this window and that EED was required to repress these genes in GV oocytes. This transient activity of PRC2 facilitated H3K27me3 establishment on a wide range of *Eed* oocyte DEGs immediately prior to DNMT3L upregulation, indicating that EED-dependent programming precedes *de novo* DNA methylation and that epigenetic programming is highly temporally and spatially regulated during oocyte growth. As many of the same genes were marked by EED-dependent H3K27me3 in mouse and human GV oocytes, the role of PRC2 appears to be conserved in human and mouse oocytes. These findings broaden the understanding of the temporal, spatial and functional activity of PRC2 in the female germline

The *Eed* oocyte DEGs identified included five H3K27me3 imprinted and seven classically imprinted genes (three of the classically imprinted genes detected were also listed as H3K27me3 imprinted genes). However, the vast majority of *Eed* oocyte DEGs were not known imprinted loci, but included many genes known to regulate cell differentiation during fetal development. Despite this, the *Eed* oocyte DEGs identified were not over-expressed in pre-implantation offspring and lost H3K27me3 during pre-implantation development. While the significance of PRC2 regulation of these genes requires further investigation, previous studies revealed that loss of EED in the oocyte affects early development and post-natal outcomes in opposing ways: offspring from *Eed* null oocytes exhibit both placental and offspring growth restriction at E10.5 (33), but were subsequently overgrown by early post-natal stages (40). While the mechanisms remain unclear, the collective data indicate that PRC2 acts at multiple levels of oocyte growth and pre-implantation development to modulate outcomes in offspring.

In previous studies there has been a significant focus on PRC2 as a maternal factor complex that regulates aspects of pre-implantation development, including X-inactivation (31-34, 58). In this study we detected EZH2 in oocytes from the primordial follicle stage through to the SN GV oocyte stage, whereas SUZ12 and EED were only identified within primary and secondary follicle stage oocytes. Since all three components are required for PRC2 methyltransferase activity (9-12), this identifies a discrete window in primary-secondary follicle oocytes during which PRC2 has the capacity to catalyse methylation of H3K27. While proteins for EED or SUZ12 were not detected in association with chromatin of GV and MII oocytes in our study, all three proteins were robustly detected in both maternal and paternal pronuclei 12 hours post-fertilisation, highlighting a role for maternally inherited PRC2 in zygotes. As previous reports detected SUZ12, EED and EZH2 protein in MII oocytes using western blots (41, 42), it is likely that a maternal supply of protein resides in the cytoplasm but is difficult to detect using IF. However, it is also possible that maternal RNA for *Eed, Suz12* and *Ezh2* is inherited via the oocyte and is translated to facilitate enrichment of PRC2 in the maternal and paternal pronuclei of zygotes. Regardless of the mode of inheritance, these observations suggest that PRC2 has distinct activities that differentially impact epigenetic regulation in growing oocytes and affect pre-implantation development in offspring.

Consistent with this, loss of EED in the oocyte affected different genes sets in oocytes and in pre-implantation offspring. While <5% of *Eed* oocyte DEGs were imprinted genes, the vast majority were not imprinted and many were associated with post-implantation cell differentiation and tissue development. Moreover, although EED was required for repression of these genes in oocytes, very few *Eed* oocyte DEGs were dysregulated in morula and blastocysts derived from *Eed*-null oocytes, and H3K27me3 was lost on these genes during pre-implantation development. While this is consistent with previous findings that many developmental genes lose H3K27me3 during pre-implantation development (44), it also indicates that their repression at this stage does not require H3K27me3. Despite this, PRC2 is required in the oocyte for regulating a large cohort of genes in pre-implantation embryos that are distinct from the *Eed* DEGs identified here, and are dysregulated when *Eed* is deleted in oocytes. Thus, while EED is required for enriching H3K27me3 and repressing a large cohort of developmental genes in primary-secondary oocytes, it also regulates a distinct set of genes in pre-implantation embryos. Therefore, PRC2 functions both to epigenetically program a wide range of imprinted and non-imprinted genes in oocytes and acts as a maternal factor in the zygote.

Our data indicates that H3K27me3 was established in the promoters of *Eed* oocyte DEGs immediately before the onset of DNA methylation, raising the possibility that H3K27me3 could influence the establishment of other epigenetic modifications in oocytes. While H3K27me3 and DNA methylation are generally mutually exclusive (44), H3K36me3 coincides with DNA methylation in oocytes (59) and H3K36me3 deposition increases in regions that subsequently acquire DNA methylation in oocytes (60). Further, while loss of H3K36me3 in oocytes results in ectopic H3K27me3 deposition in oocytes (59), it is not known whether H3K36me3 is altered in oocytes following loss of H3K27me3. As the relationship between DNA methylation/H3K36me3 and H3K27me3 is antagonistic, a potential role of H3K27me3 in oocytes may be to act as a "place keeper" that ensures the promoters of EED-dependent oocyte genes are not subject to other forms of epigenetic alteration (Fig. 7), such as DNA methylation or H3K36 methylation (59). Such an effect may be similar to that proposed for H3K27me3 in protecting regions from DNA methylation during sperm maturation (47) and may explain both the enrichment of H3K27me3 on genes that regulate fetal development and why H3K27me3 is cleared from these genes during pre-implantation offspring development.

As transient PRC2 activity occurs early during oocyte growth and immediately precedes DNMT activity (61), it is reasonable to speculate that in the absence of H3K27me3 *Eed* oocyte DEGS may accumulate H3K36 and subsequent DNA methylation. Aberrant establishment of DNA methylation in *Eed* null oocytes may then contribute to developmental outcomes in subsequent offspring. To our knowledge, no study has directly measured the impact of maternal PRC2 deletion on global DNA methylation within the oocyte. Inoue *et al.* observed that classically imprinted gene expression was normal in maternal *Eed*-null embryos and concluded that DNA methylation establishment at classically imprinted genes was not impacted by *Eed* deletion (33). However, this does not exclude the possibility that H3K27me3 protects other regions from establishing DNA methylation in oocytes, particularly the oocyte DEGs identified in this study and other H3K27me3 enriched genes identified in other studies (33, 35, 44, 46). Further work is therefore required to determine the potential impact of H3K27me3 loss in primary-secondary oocytes on the broader epigenetic landscape of mature oocytes.

The potential for H3K27me3 to guide epigenetic state of target genes in oocytes is of interest, as using this model we previously observed post-natal overgrowth in offspring derived from oocytes lacking EED (40). However, another study showed that E10.5 embryos from *Eed*-null oocytes were growth restricted (33) indicating that loss of EED in oocytes differentially impacts embryonic and offspring growth. Placental hyperplasia has been attributed to loss of H3K27me3-dependent imprinting at a small number of genes in mice derived by SCNT (36-38), but is considered to be a placental effect. While this could lead to large offspring from oocytes lacking EED, it is yet to be observed in a model with oocyte-specific *Eed* deletion and does not explain why early embryos were smaller. One explanation could be that loss of maternal PRC2 in the zygote and early pre-implantation embryo hampers early development. However, an alternative explanation is that EED and H3K27me3-dependent programming of developmental genes in growing oocytes may also affect offspring growth and development through an as-yet undefined epigenetically inherited mechanism, such as altered DNA methylation.

Finally, previous studies have demonstrated a link between H3K27me3 and repression of repetitive sequences when DNA methylation levels are low, including in male and female fetal germ cells and embryonic stem cells (55-57). However, we did not observe any change in L1 expression in GV oocytes. With the obvious caveat that these sequences may have been repressed by other epigenetic modifications such as DNA methylation in growing oocytes, our data indicate that PRC2 is dispensable for repressing L1 sequences, and possibly other repetitive sequences in GV oocytes.

Conclusions

In summary, we provide evidence that PRC2 acts transiently to establish H3K27me3 on a wide range of developmental genes in primary-secondary follicle oocytes and that this activity is required for the repression of these genes in fully-grown oocytes. As this activity precedes DNA methylation, and loss of H3K36me3 allows inappropriate spreading of H3K27me3 in oocytes, it seems likely that loss of H3K27me3 will affect other epigenetic programming events in oocytes. Moreover, as the transient activity of PRC2 in primary to secondary oocytes is distinct from the established maternal factor activity of PRC2 in pre-implantation embryos, and different gene sets are affected in oocytes and in pre-implantation embryos, these activities of PRC2 have distinct

467 developmental consequences in offspring. Finally, as common genes are targeted for H3K27me3
468 enrichment in both mouse and human oocytes, understanding the activity of PRC2 during the
469 growth of murine oocytes is likely to provide insight not only into non-genetic inheritance, but
470 also for determining how altered PRC2 activity in oocytes affects human health.
471
472
473 **Methods**
474
475 **Mouse strains, animal care and ethics**
476 Mice were housed at Monash Medical Centre Animal Facility using a 12h light-dark cycle as
477 previously reported (40). Food and water were available *ad libitum* with room temperature
478 maintained at 21-23°C with controlled humidity. All animal work was undertaken in accordance
479 with Monash University Animal Ethics Committee (AEC) approvals. Mice were obtained from the
480 following sources: *Zp3Cre* mice (C57BL/6-Tg 93knw/J; Jackson Labs line 003651, constructed and
481 shared by Prof Barbara Knowles (62)), *Eed* floxed mice ($Eed^{fl/fl}$) (B6; 129S1-*Eed*tm1Sho/J; Jackson
482 Labs line 0022727; constructed and shared by Prof Stuart Orkin *(63)*. The *Eed* line was backcrossed
483 to a pure C57BL6/J and shared with us by Associate Professor Rhys Allen and Professor Marnie
484 Blewitt, Walter and Eliza Hall Institute for Medical Research, Melbourne.
485
486 **Genotyping**
487 All animals were genotyped via ear punch at weaning by Transnetyx (Cordova, TN) using real-time
488 PCR assays (details available upon request) designed for each gene as described previously (40).
489
490 **Collection, antibody incubation and detection of ovaries for immunofluorescence**
491 Ovaries for immunofluorescence (IF) were fixed in 4% paraformaldehyde (PFA) overnight at 4°C.
492 Samples were then washed in PBS and processed through 70% ethanol and embedded in paraffin
493 blocks, sectioned at 5µm and transferred to Superfrost™ Plus slides (Thermo-Fisher). Antigen
494 retrieval was performed using DAKO Citrate buffer (pH 6.0) at 98°C for 30 minutes and non-
495 specific binding blocked in PBS containing 5% BSA and 10% donkey serum for 1h at RT. Blocking
496 solution was replaced with PBS containing 0.1% Triton-X 100 (PBSTX) and appropriately diluted
497 primary antibodies (Supp. Materials and Methods) and incubated overnight at 4°C. Slides were
498 washed in PBS and incubated with PBSTX containing secondary antibody for 1h at RT. After final
499 washes in PBS, slides were rinsed in distilled H2O, mounted in DAPI ProLong Gold® and dried

overnight. Fluorescence was detected using the VS120 Slide Scanner and quantified using QuPath Image Analysis Software (QuPath). Background fluorescence in the oocyte cytoplasm was removed from nuclear intensity. When comparing control versus experimental groups, the control mean was set to 1.0.

Collection of oocytes and pre-implantation embryos for immunofluorescence

Ovaries were punctured using 30 G needles to release oocytes. GV oocytes were partially denuded mechanically using a narrow-bore glass pipette. For MII oocyte and zygote collections, females were injected with 5 international units (IU) Pregnant Mare Serum Gonadotropin (PMSG) followed by Human Chorionic Gonadotropin (hCG; 48h interval) and in the case of zygote collections were bred to C57BL/6 males. MII oocytes or zygotes were removed from the ampulla, denuded in M2 media containing hyaluronidase (0.3 mg/ml). Samples were either frozen and used for RNA analysis or fixed in 4% PFA containing 2% Triton X-100 for 30 minutes at RT. Samples were then washed in PBS containing 0.1% Tween, 0.01% Triton X-100 and 1% BSA (PBST-BSA) and stored in PBST-BSA.

Oocyte and zygote whole-mount immunofluorescence

GV, MII oocytes and zygotes were blocked in PBST-BSA containing 10% donkey serum for 1 hour (h) at RT. The solution was then replaced with PBST-BSA containing appropriately diluted primary antibodies (Supp. Materials and Methods) and incubated overnight (o/n) at 4°C. Samples were washed in PBST-BSA and then incubated in PBST-BSA containing secondary antibodies (Supp. Materials and Methods) for 4h (GVs) or 1h (MII and zygote) in the dark at RT. After washing with PBST-BSA, samples were incubated with Hoechst 33342 (500 µg/ml) or DAPI (100 µg/ml) for 1h at RT, washed and stored in PBST-BSA until imaging. Fluorescence was detected using the Nikon C1 inverted confocal microscope and signal intensity quantified using ImageJ. Background fluorescence levels were measured in the cytoplasm and removed from nuclear intensity, with control mean was set to 1.0 for comparisons.

Collection of oocyte RNA and RNA-sequencing

Cumulus-Oocyte Complexes (COCs) were collected from eight to twelve-week-old female mice and transferred to M2 media. Oocytes were denuded mechanically with a narrow-bore glass pipette and incubated with M2 media containing 5 µg/mL Hoechst 33342 for 10 minutes at 37°C.

GV oocytes were then scored as either surrounded nucleolus (SN), or non-surrounded nucleolus (NSN) based on Hoechst staining. SN oocytes were then collected, frozen on dry ice and stored at -80°C until RNA extraction. Ten to fifteen oocytes isolated from each female were pooled and total RNA isolated using the Agencourt RNAdvance Cell V2 extraction kit. High quality RNA (RIN >7.5) was used for library preparation (>1.2ng total RNA) using the Nugen Trio Library protocol, MU01440V2; 2017. 75bp single end sequencing was carried out on 4-6 libraries / genotype using Illumina NextSeq500 High output mode and v2.5 chemistry (Illumina Protocol 15046563 v02, Mar 2016) to collect >25M reads per sample.

RNA-sequencing data analyses

Adaptor and low quality sequences in raw sequencing reads were trimmed either using AdaptorRemovel (64) (v2.2.1) for the oocyte RNA-Seq dataset with the following parameters: --trimns -- trimqualities --minquality 20 --minlength 35, or using Trimmomatic (65) (v0.39) for bone growth plate and placental RNA-Seq datasets with the following parameters: LEADING:3 TRAILING:3 SLIDINGWINDOW:4:15 MINLEN:20. Clean reads were mapped to the mouse reference genome (GRCm38) using either STAR (66) (v2.5.3a) for the oocyte RNA-Seq dataset with default settings, or STAR (v2.7.5c) for the bone growth plate and placental RNA-Seq datasets with following settings: outFilterMismatchNoverLmax 0.03 --alignIntronMax 10000. For oocyte RNA-Seq dataset, raw counts for mouse reference genes (ensembl-release-93) were calculated using featureCounts (67) (v1.5.2) based on mapped bam files with the following parameters: -Q 10 -s 2. For bone growth plate and placental RNA-Seq datasets, raw counts for mouse reference genes (ensembl-release-101) were calculated using STAR (v2.7.5c) with parameter "--quantMode GeneCounts". Raw counts of technical replicates from different sequencing lanes for the same samples in bone growth plate RNA-Seq dataset were merged. Differential gene expression analysis was carried out using R package “limma” (68) with “treat” function with parameter as “lfc=log(1.2)” for the oocyte RNA-Seq dataset or “lfc=log(1.1)” for the bone growth plate and placental RNA-Seq datasets. Statistically significantly differentially expressed genes were identified using “FDR < 0.05”. Gene Ontology (GO) enrichment analysis for significantly differentially expressed genes was carried out using The Database for Annotation, Visualisation and Integrated Discovery (DAVID) with following settings: GO term level 3, minimum gene count 5, and FDR < 0.05 (69).

Analyses of genome-wide H3K27me3 distribution and H3K27me3 datasets in oocytes

Eed GV DEGs were compared to publicly available H3K27me3 ChIP-seq, CUT & RUN and CUT & TAG datasets of oocytes, sperm and pre-implantation embryos. Datasets used are summarised in Supp. Materials and Methods.

For the dataset from Zheng *et al.* 2016 (GSE76687), processed files including whole genome scale broad H3K27me3 peaks were downloaded and used for the comparison (44). For the dataset from Liu *et al.* 2016 (GSE73952), H3K27me3 states of the promoter regions of mouse reference genes were retrieved from Table S1 of the paper and used for the comparison (46). For the dataset from Erkek *et al.* 2013 (GSE42629), raw sequencing data were downloaded and then adaptor and low-quality sequences were trimmed using bbduk (v38.94) (47). Clean reads were mapped to the mouse reference genome (mm9) using bowtie2(70) (v2.4.4) with default settings. H3K27me3 peaks were identified using MACS2(71) (v2.1.1) with the following parameters: -g 1.87e9 --nomodel --broad -q 0.05. For the dataset from Inoue *et al.* 2018 (GSE116713), bigwig format files were downloaded and converted to bedGraph format using "bigWigToBedGraph" from UCSC utilities, and then H3K27me3 peaks were called using MACS2 (v2.1.1) based on the bedGraph files with the following parameter: -c 1.3 (equivalent to P value < 0.05) (33). For the human dataset from Xia *et al.* 2019 (GSE124718), processed files including whole genome scale broad H3K27me3 peaks were downloaded and used for the comparison (48).

This comparison took the 349 *Eed* GV DEGs and asked whether their promoters (defined as 2Kb up- or down-stream of TSS to be consistent with Liu *et al.* 2016) overlapped with H3K27me3 peaks (> 200bp overlap) in the above mentioned publicly available H3K27me3 ChIP or CUT & RUN datasets. For the human dataset from Xia *et al*. 2019 (GSE124718), human orthologous genes of mouse 349 *Eed* GV DEGs were identified and used for the comparison.

Statistical Analyses

GraphPad Prism 9 was used for statistical analysis and to graph datasets. As appropriate, parametric Student's *t* tests or ANOVA or non-parametric equivalents as indicated in figure legends.

Declarations

Ethics approval and consent to participate:

All animal work was undertaken in accordance with Monash University Animal Ethics Committee (AEC) approvals.

Consent for publication:

Not applicable

Availability of data and materials

All RNA sequencing data have been deposited to the Gene Expression Omnibus (GEO) and are publicly available with accession number GSE193582. All other information is available from the corresponding author.

Competing interests:

The authors declare that they have no competing interests that affect this work

Funding:

This work was supported by grants and research funding from:
National Health and Medical Research Project Grant GNT1144966 (PSW, DKG, MvdB, DLA)
Hudson Institute of Medical Research (PSW)
Victorian Government's Operational Infrastructure Support Program.
Monash University Postgraduate Student Awards (EGJ, RO and SP)

Author contributions:

Conceived and/or designed experiments/interpreted outcomes: EGJ, TT, ZQ, RO, SP, WTG, DLA, PSW
Performed experiments and/or analysed data: EGJ, ZQ, TT, RO, SP, HB, QZ, JMS, DLA, PSW
Bioinformatic analyses and/or comparisons with published datasets: ZQ, EGJ, SMP, DLA, PSW
Resources and/or supervision PSW DKG, MvdB, DLA, JC, NAS
Writing - original draft: EGJ, PSW, ZQ, RO, SP, NAS, DLA
Writing - review & editing: EGJ, PSW, RO, SP, DLA. All authors critically read and approved the manuscript.

Competing interests: The authors declare that they have no competing interests.

Data and materials availability: With exception of the RNA sequencing data generated in this study, all data are available in the main text, the Supplementary Materials. The RNA sequencing data have been deposited in the Gene Expression Omnibus (GEO) and are publicly available with accession number GSE193582. Published datasets used in this study are summarised in the Supplementary materials.

Acknowledgments:

We thank Dr. Neil Youngson and Prof. Marnie Blewitt for critical comments on the manuscript, Monash Animal Research Platform staff for assistance with mouse care, Monash Histology Platform for assistance with slide scanning and the Monash Micro Imaging Facility and MHTP Medical Genomics Facilities for assistance and technical advice.

References

1. Esteller M. Epigenetics in cancer. N Engl J Med. 2008;358(11):1148-59.
2. Sharma S, Kelly TK, Jones PA. Epigenetics in cancer. Carcinogenesis. 2010;31(1):27-36.
3. Rosen ED, Kaestner KH, Natarajan R, Patti M-E, Sallari R, Sander M, et al. Epigenetics and Epigenomics: Implications for Diabetes and Obesity. Diabetes. 2018;67(10):1923.
4. Tran NQV, Miyake K. Neurodevelopmental Disorders and Environmental Toxicants: Epigenetics as an Underlying Mechanism. Int J Genom. 2017;2017:7526592.
5. Ferguson-Smith AC. Genomic imprinting: the emergence of an epigenetic paradigm. Nat Rev Genet. 2011;12:565.
6. Barlow DP, Bartolomei MS. Genomic Imprinting in Mammals. Cold Spring Harb Perspect Biol. 2014;6(2).
7. Stewart KR, Veselovska L, Kelsey G. Establishment and functions of DNA methylation in the germline. Epigenomics. 2016;8(10):1399-413.
8. Hanna CW, Kelsey G. Features and mechanisms of canonical and noncanonical genomic imprinting. Genes Dev. 2021;35(11-12):821-34.
9. Pasini D, Bracken AP, Jensen MR, Denchi EL, Helin K. Suz12 is essential for mouse development and for EZH2 histone methyltransferase activity. EMBO J. 2004;23(20):4061-71.
10. Faust C, Schumacher A, Holdener B, Magnuson T. The eed mutation disrupts anterior mesoderm production in mice. Development. 1995;121(2):273-85.
11. O'Carroll D, Erhardt S, Pagani M, Barton SC, Surani MA, Jenuwein T. The polycomb-group gene Ezh2 is required for early mouse development. Mol Cell Biol. 2001;21(13):4330-6.
12. Shen X, Liu Y, Hsu YJ, Fujiwara Y, Kim J, Mao X, et al. EZH1 mediates methylation on histone H3 lysine 27 and complements EZH2 in maintaining stem cell identity and executing pluripotency. Mol Cell. 2008;32(4):491-502.
13. He A, Shen X, Ma Q, Cao J, von Gise A, Zhou P, et al. PRC2 directly methylates GATA4 and represses its transcriptional activity. Genes Dev. 2012;26(1):37-42.
14. Lee JM, Lee JS, Kim H, Kim K, Park H, Kim JY, et al. EZH2 generates a methyl degron that is recognized by the DCAF1/DDB1/CUL4 E3 ubiquitin ligase complex. Mol Cell. 2012;48(4):572-86.
15. Su IH, Dobenecker MW, Dickinson E, Oser M, Basavaraj A, Marqueron R, et al. Polycomb group protein ezh2 controls actin polymerization and cell signaling. Cell. 2005;121(3):425-36.
16. Gunawan M, Venkatesan N, Loh JT, Wong JF, Berger H, Neo WH, et al. The methyltransferase Ezh2 controls cell adhesion and migration through direct methylation of the extranuclear regulatory protein talin. Nat Immunol. 2015;16(5):505-16.
17. Vasanthakumar A, Xu D, Lun AT, Kueh AJ, van Gisbergen KP, Iannarella N, et al. A non-canonical function of Ezh2 preserves immune homeostasis. EMBO Rep. 2017;18(4):619-31.
18. Wang J, Wang GG. No Easy Way Out for EZH2: Its Pleiotropic, Noncanonical Effects on Gene Regulation and Cellular Function. Int J Mol Sci. 2020;21(24).
19. Koyen AE, Madden MZ, Park D, Minten EV, Kapoor-Vazirani P, Werner E, et al. EZH2 has a non-catalytic and PRC2-independent role in stabilizing DDB2 to promote nucleotide excision repair. Oncogene. 2020;39(25):4798-813.
20. Boyer LA, Plath K, Zeitlinger J, Brambrink T, Medeiros LA, Lee TI, et al. Polycomb complexes repress developmental regulators in murine embryonic stem cells. Nature. 2006;441(7091):349-53.

21. Cohen AS, Gibson WT. EED-associated overgrowth in a second male patient. J Hum Genet. 2016;61(9):831-4.
22. Cohen AS, Tuysuz B, Shen Y, Bhalla SK, Jones SJ, Gibson WT. A novel mutation in EED associated with overgrowth. J Hum Genet. 2015;60(6):339-42.
23. Cooney E, Bi W, Schlesinger AE, Vinson S, Potocki L. Novel EED mutation in patient with Weaver syndrome. American journal of medical genetics Part A. 2017;173(2):541-5.
24. Imagawa E, Higashimoto K, Sakai Y, Numakura C, Okamoto N, Matsunaga S, et al. Mutations in genes encoding polycomb repressive complex 2 subunits cause Weaver syndrome. Hum Mutat. 2017;38(6):637-48.
25. Tatton-Brown K, Hanks S, Ruark E, Zachariou A, Duarte Sdel V, Ramsay E, et al. Germline mutations in the oncogene EZH2 cause Weaver syndrome and increased human height. Oncotarget. 2011;2(12):1127-33.
26. Tatton-Brown K, Loveday C, Yost S, Clarke M, Ramsay E, Zachariou A, et al. Mutations in Epigenetic Regulation Genes Are a Major Cause of Overgrowth with Intellectual Disability. Am J Hum Genet. 2017;100(5):725-36.
27. Gibson WT, Hood RL, Zhan SH, Bulman DE, Fejes AP, Moore R, et al. Mutations in EZH2 cause Weaver syndrome. Am J Hum Genet. 2012;90(1):110-8.
28. Cohen AS, Yap DB, Lewis ME, Chijiwa C, Ramos-Arroyo MA, Tkachenko N, et al. Weaver Syndrome-Associated EZH2 Protein Variants Show Impaired Histone Methyltransferase Function In Vitro. Hum Mutat. 2016;37(3):301-7.
29. Cyrus SS, Cohen ASA, Agbahovbe R, Avela K, Yeung KS, Chung BHY, et al. Rare SUZ12 variants commonly cause an overgrowth phenotype. Am J Med Genet C Semin Med Genet. 2019;181(4):532-47.
30. Imagawa E, Albuquerque EVA, Isidor B, Mitsuhashi S, Mizuguchi T, Miyatake S, et al. Novel SUZ12 mutations in Weaver-like syndrome. Clin Genet. 2018;94(5):461-6.
31. Erhardt S, Su IH, Schneider R, Barton S, Bannister AJ, Perez-Burgos L, et al. Consequences of the depletion of zygotic and embryonic enhancer of zeste 2 during preimplantation mouse development. Development. 2003;130(18):4235-48.
32. Inoue A, Jiang L, Lu F, Zhang Y. Genomic imprinting of Xist by maternal H3K27me3. Genes Dev. 2017;31(19):1927-32.
33. Inoue A, Chen Z, Yin Q, Zhang Y. Maternal Eed knockout causes loss of H3K27me3 imprinting and random X inactivation in the extraembryonic cells. Genes Dev. 2018;32(23-24):1525-36.
34. Harris C, Cloutier M, Trotter M, Hinten M, Gayen S, Du Z, et al. Conversion of random X-inactivation to imprinted X-inactivation by maternal PRC2. eLife. 2019;8:e44258.
35. Inoue A, Jiang L, Lu F, Suzuki T, Zhang Y. Maternal H3K27me3 controls DNA methylation-independent imprinting. Nature. 2017;547:419.
36. Inoue K, Ogonuki N, Kamimura S, Inoue H, Matoba S, Hirose M, et al. Loss of H3K27me3 imprinting in the Sfmbt2 miRNA cluster causes enlargement of cloned mouse placentas. Nat Commun. 2020;11(1):2150.
37. Wang L-Y, Li Z-K, Wang L-B, Liu C, Sun X-H, Feng G-H, et al. Overcoming Intrinsic H3K27me3 Imprinting Barriers Improves Post-implantation Development after Somatic Cell Nuclear Transfer. Cell Stem Cell. 2020;27(2):315-25.e5.
38. Xie Z, Zhang W, Zhang Y. Loss of Slc38a4 imprinting is a major cause of mouse placenta hyperplasia in somatic cell nuclear transferred embryos at late gestation. Cell Rep. 2022;38(8):110407.

39. Chen Z, Zhang Y. Maternal H3K27me3-dependent autosomal and X chromosome imprinting. Nat Rev Genet. 2020;21(9):555-71.
40. Prokopuk L, Stringer J, White R, Vossen R, White S, Cohen A, et al. Loss of maternal EED results in postnatal overgrowth. Clin Epigenetics. 2018;10(1):95.
41. Puschendorf M, Terranova R, Boutsma E, Mao X, Isono K-i, Brykczynska U, et al. PRC1 and Suv39h specify parental asymmetry at constitutive heterochromatin in early mouse embryos. Nat Genet. 2008;40(4):411-20.
42. Qu Y, Lu D, Jiang H, Chi X, Zhang H. EZH2 is required for mouse oocyte meiotic maturation by interacting with and stabilizing spindle assembly checkpoint protein BubRI. Nucleic Acids Res. 2016;44(16):7659-72.
43. Wang H, Paulson EE, Ma L, Ross PJ, Schultz RM. Paternal genome rescues mouse preimplantation embryo development in the absence of maternally-recruited EZH2 activity. Epigenetics. 2019;14(1):94-108.
44. Zheng H, Huang B, Zhang B, Xiang Y, Du Z, Xu Q, et al. Resetting Epigenetic Memory by Reprogramming of Histone Modifications in Mammals. Mol Cell. 2016;63(6):1066-79.
45. Lewandoski M, Wassarman KM, Martin GR. Zp3-cre, a transgenic mouse line for the activation or inactivation of loxP-flanked target genes specifically in the female germ line. Curr Biol. 1997;7(2):148-51.
46. Liu X, Wang C, Liu W, Li J, Li C, Kou X, et al. Distinct features of H3K4me3 and H3K27me3 chromatin domains in pre-implantation embryos. Nature. 2016;537(7621):558-62.
47. Erkek S, Hisano M, Liang CY, Gill M, Murr R, Dieker J, et al. Molecular determinants of nucleosome retention at CpG-rich sequences in mouse spermatozoa. Nat Struct Mol Biol. 2013;20(7):868-75.
48. Xia W, Xu J, Yu G, Yao G, Xu K, Ma X, et al. Resetting histone modifications during human parental-to-zygotic transition. Science. 2019;365(6451):353.
49. Andergassen D, Dotter CP, Wenzel D, Sigl V, Bammer PC, Muckenhuber M, et al. Mapping the mouse Allelome reveals tissue-specific regulation of allelic expression. eLife. 2017;6:e25125.
50. Wanigasuriya I, Gouil Q, Kinkel SA, Tapia del Fierro A, Beck T, Roper EA, et al. Smchd1 is a maternal effect gene required for genomic imprinting. eLife. 2020;9:e55529.
51. Sugimoto M, Abe K. X chromosome reactivation initiates in nascent primordial germ cells in mice. PLoS Genet. 2007;3(7):e116.
52. Chuva de Sousa Lopes SM, Hayashi K, Shovlin TC, Mifsud W, Surani MA, McLaren A. X chromosome activity in mouse XX primordial germ cells. PLoS Genet. 2008;4(2):e30.
53. Talon I, Janiszewski A, Chappell J, Vanheer L, Pasque V. Recent Advances in Understanding the Reversal of Gene Silencing During X Chromosome Reactivation. Front Cell Dev Biol. 2019;7.
54. Prokopuk L, Stringer JM, Hogg K, Elgass KD, Western PS. PRC2 is required for extensive reorganization of H3K27me3 during epigenetic reprogramming in mouse fetal germ cells. Epigenetics Chromatin. 2017;10(7).
55. Stringer JM, Forster SC, Qu Z, Prokopuk L, O'Bryan MK, Gardner DK, et al. Reduced PRC2 function alters male germline epigenetic programming and paternal inheritance. BMC Biol. 2018;16(1):104.
56. Huang T-C, Wang Y-F, Vazquez-Ferrer E, Theofel I, Requena CE, Hanna CW, et al. Sex-specific chromatin remodelling safeguards transcription in germ cells. Nature. 2021;600(7890):737-42.

57. Walter M, Teissandier A, Perez-Palacios R, Bourc'his D. An epigenetic switch ensures transposon repression upon dynamic loss of DNA methylation in embryonic stem cells. eLife. 2016;5:e11418.
58. Chen Z, Yin Q, Inoue A, Zhang C, Zhang Y. Allelic H3K27me3 to allelic DNA methylation switch maintains noncanonical imprinting in extraembryonic cells. Sci Adv. 2019;5(12):eaay7246.
59. Xu Q, Xiang Y, Wang Q, Wang L, Brind'Amour J, Bogutz AB, et al. SETD2 regulates the maternal epigenome, genomic imprinting and embryonic development. Nat Genet. 2019;51(5):844-56.
60. Stewart KR, Veselovska L, Kim J, Huang J, Saadeh H, Tomizawa S-i, et al. Dynamic changes in histone modifications precede de novo DNA methylation in oocytes. Genes Dev. 2015;29(23):2449-62.
61. Lucifero D, La Salle S, Bourc'his D, Martel J, Bestor TH, Trasler JM. Coordinate regulation of DNA methyltransferase expression during oogenesis. BMC Dev Biol. 2007;7(1):36.
62. de Vries WN, Binns LT, Fancher KS, Dean J, Moore R, Kemler R, et al. Expression of Cre recombinase in mouse oocytes: a means to study maternal effect genes. Genesis 2000;26(2):110-2.
63. Yu M, Riva L, Xie H, Schindler Y, Moran TB, Cheng Y, et al. Insights into GATA-1-mediated gene activation versus repression via genome-wide chromatin occupancy analysis. Mol Cell. 2009;36(4):682-95.
64. Schubert M, Lindgreen S, Orlando L. AdapterRemoval v2: rapid adapter trimming, identification, and read merging. BMC Res Notes. 2016;9(1):88.
65. Bolger AM, Lohse M, Usadel B. Trimmomatic: a flexible trimmer for Illumina sequence data. Bioinformatics. 2014;30(15):2114-20.
66. Dobin A, Davis CA, Schlesinger F, Drenkow J, Zaleski C, Jha S, et al. STAR: ultrafast universal RNA-seq aligner. Bioinformatics. 2013;29(1):15-21.
67. Liao Y, Smyth GK, Shi W. featureCounts: an efficient general purpose program for assigning sequence reads to genomic features. Bioinformatics. 2014;30(7):923-30.
68. Ritchie ME, Phipson B, Wu D, Hu Y, Law CW, Shi W, et al. limma powers differential expression analyses for RNA-sequencing and microarray studies. Nucleic Acids Res. 2015;43(7):e47-e.
69. Dennis G, Jr., Sherman BT, Hosack DA, Yang J, Gao W, Lane HC, et al. DAVID: Database for Annotation, Visualization, and Integrated Discovery. Genome biology. 2003;4(5):P3.
70. Langmead B, Salzberg SL. Fast gapped-read alignment with Bowtie 2. Nat Methods. 2012;9(4):357-9.
71. Zhang Y, Liu T, Meyer CA, Eeckhoute J, Johnson DS, Bernstein BE, et al. Model-based Analysis of ChIP-Seq (MACS). Genome Biol. 2008;9(9):R137.

Figures:

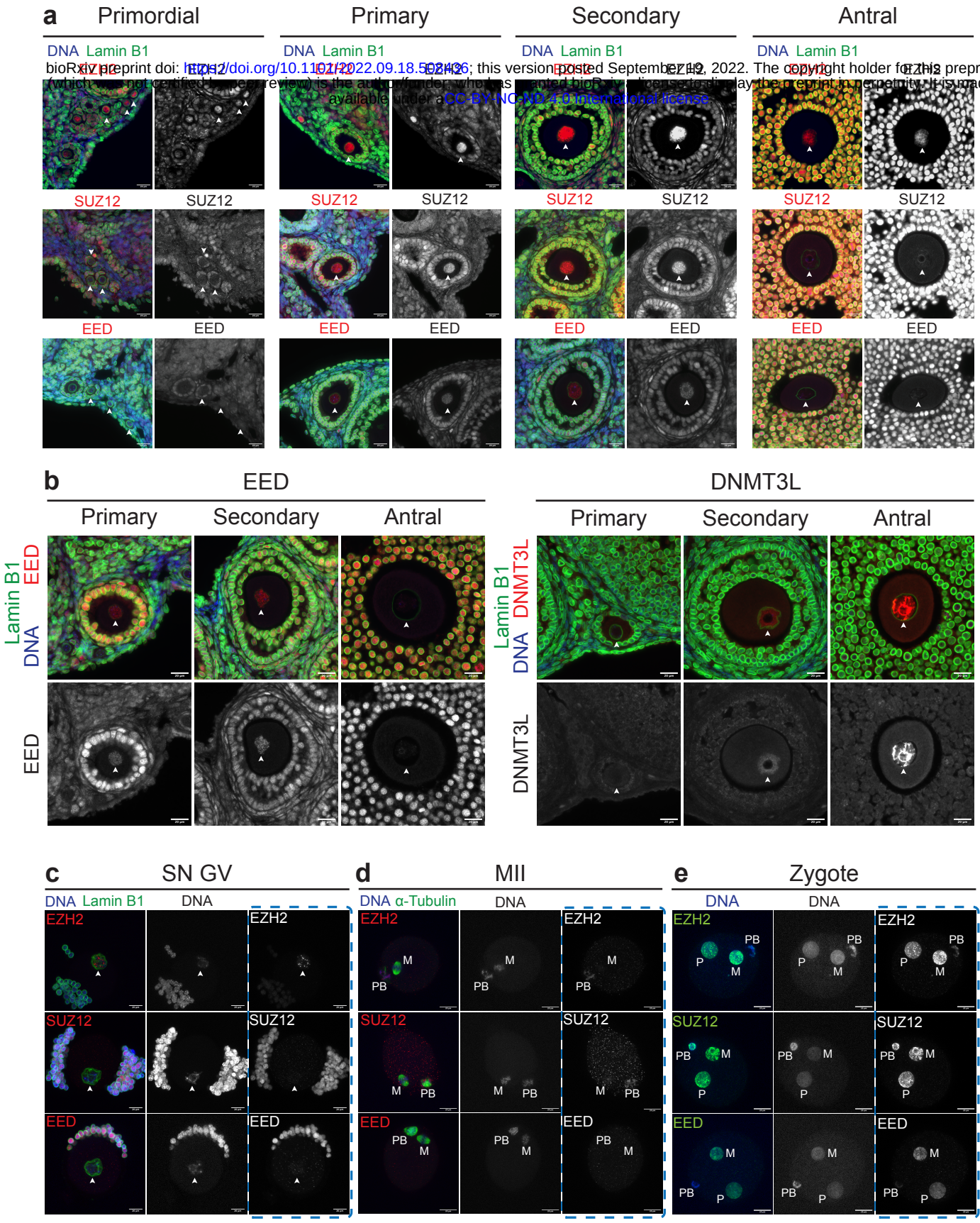

Fig 1

827 **Fig 1. PRC2 acts transiently within primary and secondary follicle growing oocytes**. **(a-d)**
828 Representative images of EZH2, SUZ12 and EED (red) IF analysis in **(a)** primordial, primary,
829 secondary and antral follicles. **(b)** Comparison of EED (red, left panels) versus DNMT3L (red, right
830 panels) IF analysis in primary, secondary and antral follicles. **(c)** Surrounded nucleolus (SN) GV
831 oocytes. **(d)** MII oocytes. α-Tubulin (green) identifies meiotic spindles. M: metaphase plate, PB:
832 polar body. **(e)** Zygotes 12h after fertilisation for ≥ 10 zygotes imaged per antibody combination.
833 M: maternal pronucleus, P: paternal pronucleus, PB: polar body. In **a-c** white arrowheads indicate
834 the oocyte nucleus defined by Lamin B1 (green) and DAPI (blue) shows DNA. In **c-e** images
835 represent compressed z-stack images of wholemount oocytes or zygotes. Scale bars: 20 μm.
836 Images in **a** and **b** are representative of two ovaries from three separate females and in **c-e** images
837 are representative of ≥10 oocytes per antibody combination.
838

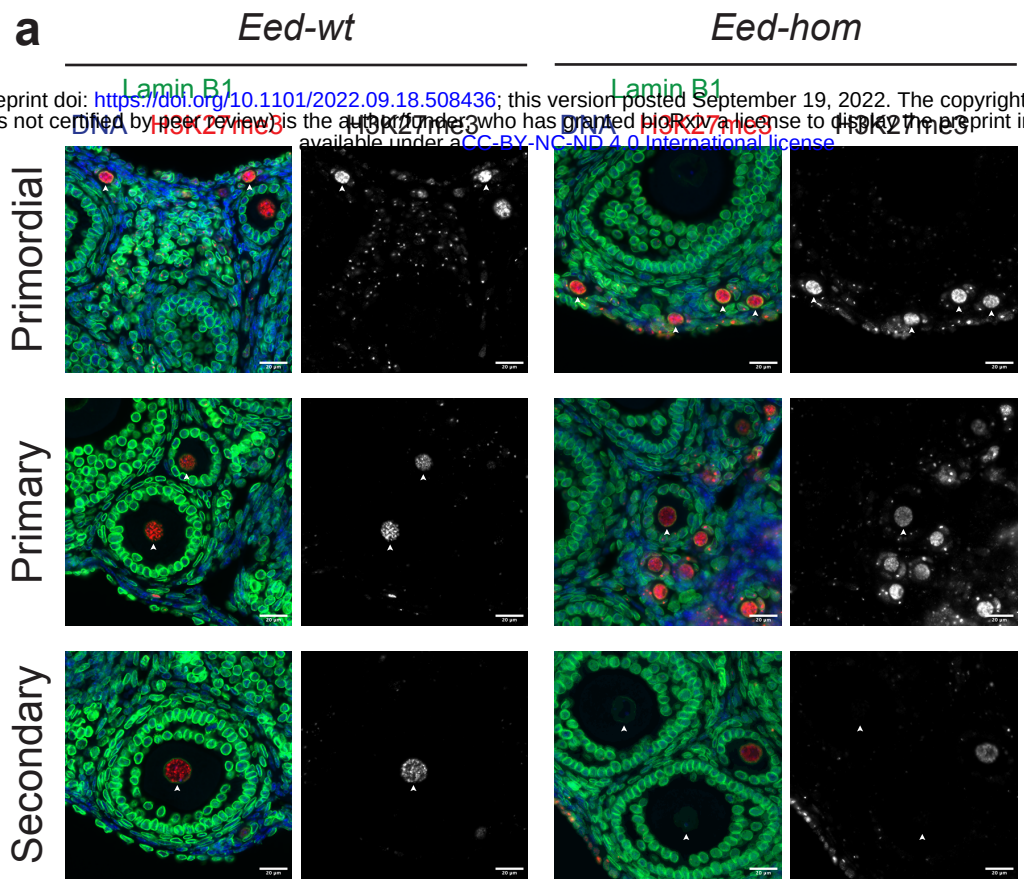

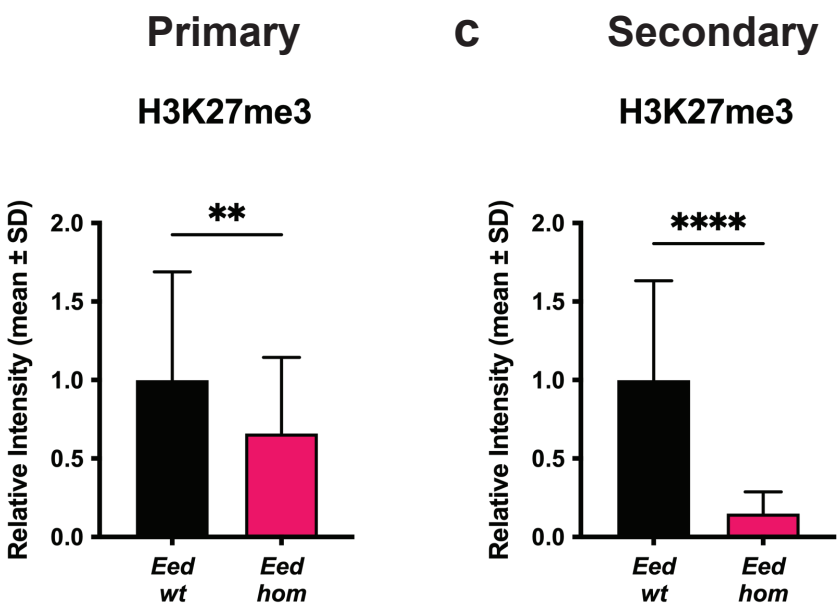

Fig 2

839 **Fig 2. Deletion of *Eed* in oocytes reduced H3K27me3 in oocytes of primary and secondary**
840 **follicles. (a)** Representative images of H3K27me3 (red) immunostaining analysis in primordial
841 (top), primary (middle) and secondary (bottom) follicle oocytes from *Eed-wt* and *Eed-hom*
842 females. White arrowheads indicate the oocyte nucleus as defined by Lamin B1 (green). DAPI
843 (blue) shows DNA in somatic cells. Images are representative of two ovaries from three biological
844 replicates. Scale bars: 20 µm. **(b-c)** Quantification of H3K27me3 within oocyte nuclei of primary
845 **(b)** and secondary **(c)** follicles from *Eed-wt* and *Eed-hom* females. Average intensity of *Eed-wt* was
846 set to 1.0. ***P* < 0.005, two-tailed Mann-Whitney U test, N = 63 *Eed-wt* and 67 *Eed-hom* primary
847 follicle oocytes. *****P* < 0.0001, two-tailed Mann-Whitney U test, N = 45 *Eed-wt* and 47 *Eed-hom*
848 secondary follicle oocytes. Error bars represent mean ± standard deviation.
849

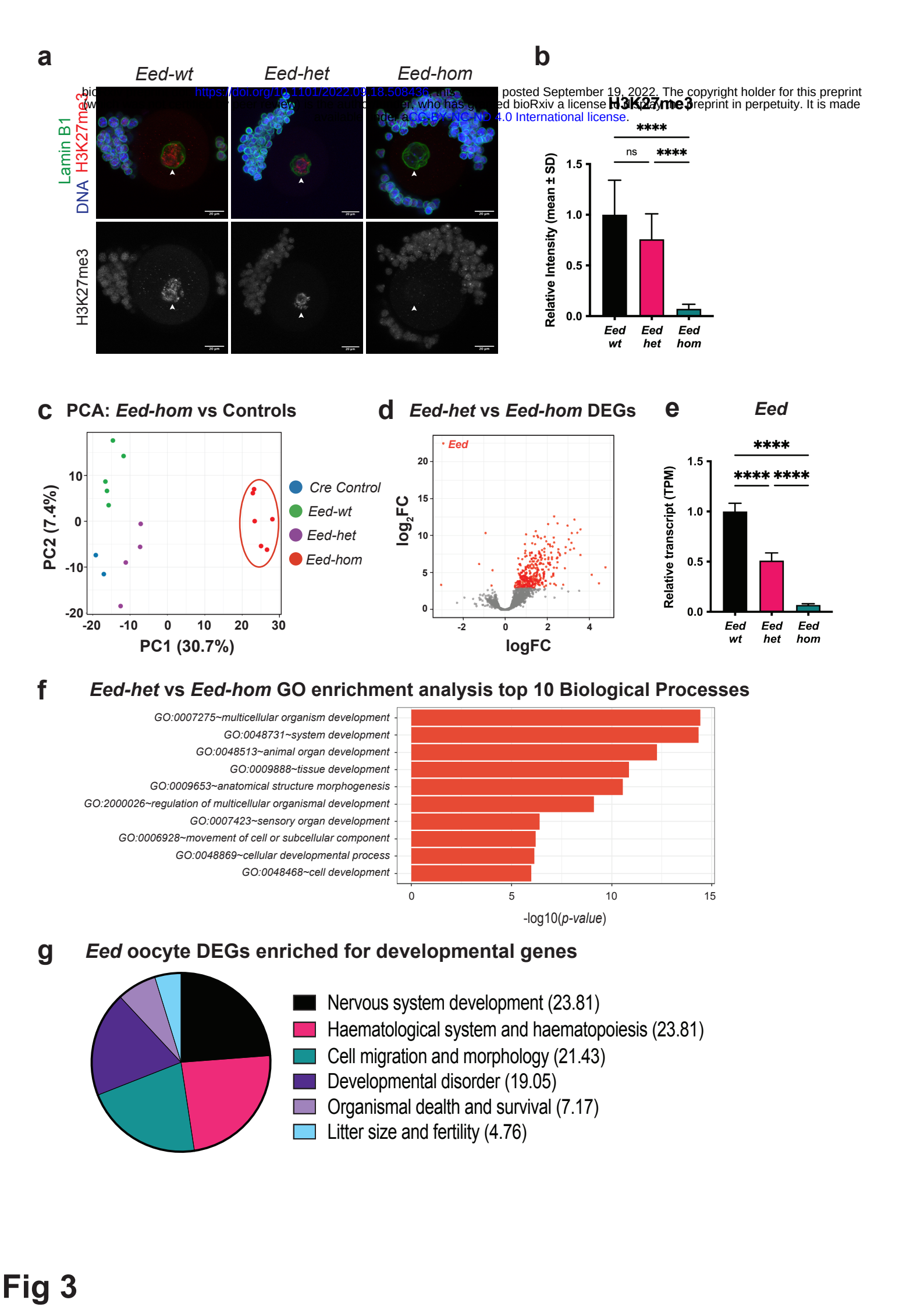

Fig 3

Fig 3. *Eed* is required for H3K27me3 establishment and developmental gene silencing in growing oocytes. (a,b) Representative images **(a)** and quantification **(b)** of H3K27me3 (red) IF in *Eed-wt*, *Eed-het*, and *Eed-hom* SN GV oocytes. White arrowheads indicate the oocyte nucleus as defined by Lamin B1 (green). DAPI (blue) shows DNA in somatic cells. Images represent 3-4 females per genotype, with 16-21 oocytes imaged per genotype. Scale bars: 20 μm. Average intensity of *Eed-wt* was set to 1.0. ****$P < 0.0001$, Kruskall-Wallis test plus Dunn's multiple comparisons test, error bars represent mean ± standard deviation. **(c)** Principal Component Analysis (PCA) of RNAseq data for *Eed-hom* (n=6) vs *Eed-het* (n=4), *Eed-wt* (n=5) and *Eed-wt Cre* (n=2) controls. **(d)** Differential gene expression analysis of *Eed-het* vs *Eed-hom* oocytes represented by volcano plot showing logFC against statistical significance. Genes with FDR-adjusted $P < 0.05$ are coloured in red. Deletion of *Eed* resulted in 349 significant DEGs (*Eed* oocyte DEGs), with 343 genes upregulated and 6 genes downregulated, including *Eed*. **(e)** Relative *Eed* transcript levels (transcripts per million reads; TPM) in *Eed-wt*, *Eed-het* and *Eed-hom* GV oocytes. Average expression of *Eed-wt* was set to 1.0. **(f)** GO enrichment analysis of *Eed* oocyte DEGs representing the top 10 significantly different biological processes impacted. **(f)** Pie chart displaying the proportion of significant pathways identified using Ingenuity pathway analysis

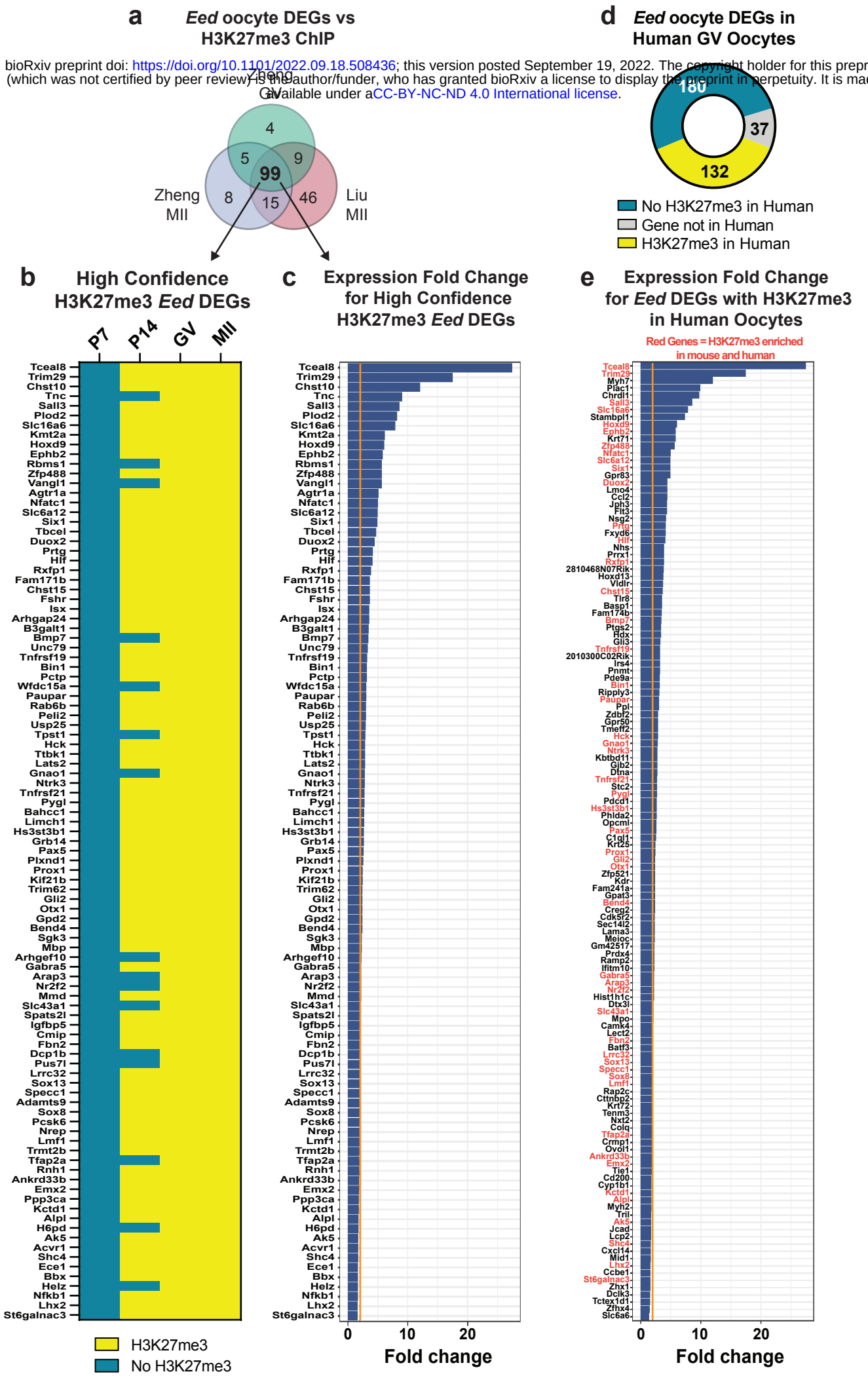

Fig 4

868 **Fig 4. H3K27me3 is established on *Eed* oocyte DEGs in primary – secondary mouse oocytes and**
869 **is conserved in human GV oocytes (a)** Venn diagram showing *Eed* oocyte DEGs that contained
870 H3K27me3 promoter peaks in GV and MII oocyte H3K27me3 ChIP-seq datasets (44, 46)
871 identifying 99 'high confidence' H3K27me3 enriched *Eed* oocyte DEGs. **(b)** Heat map showing
872 promoter H3K27me3 enrichment status of 99 high confidence H3K27me3 enriched *Eed* oocyte
873 DEGs identified in P7, P14, GV and MII oocyte H3K27me3 ChIP-seq datasets from Liu *et al*., and
874 Zheng *et al.,* (44, 46). Blue: No H3K27me3 peaks, yellow: indicates presence of H3K27me3 peaks.
875 **(c)** Expression fold change of the 99 high confidence H3K27me3 enriched *Eed* oocyte DEGs in *Eed-*
876 *hom* oocytes relative to *Eed-het.* Orange line indicates two-fold change **(d)** Donut chart showing
877 the promoter H3K27me3 enrichment status of *Eed* oocyte DEGs in Human GV oocytes (48). Grey:
878 Not conserved in humans, blue: no H3K27me3 peaks in promoter, yellow: H3K27me3 peak
879 present in promoter. **(e)** Expression fold change of 132 mouse *Eed* oocyte DEGs that were
880 H3K27me3 enriched in human GV oocytes. *Eed* oocyte DEGs commonly enriched for H3K27me3
881 in human and mouse GV oocytes are marked with genes names in red. Orange line indicates two-
882 fold change. For **(a,b and d)**, promoter region was defined as 2000bp upstream and downstream
883 of TSS, overlap of > 200bp H3K27me3 peaks with the promoter region was considered H3K27me3
884 enriched.
885
886

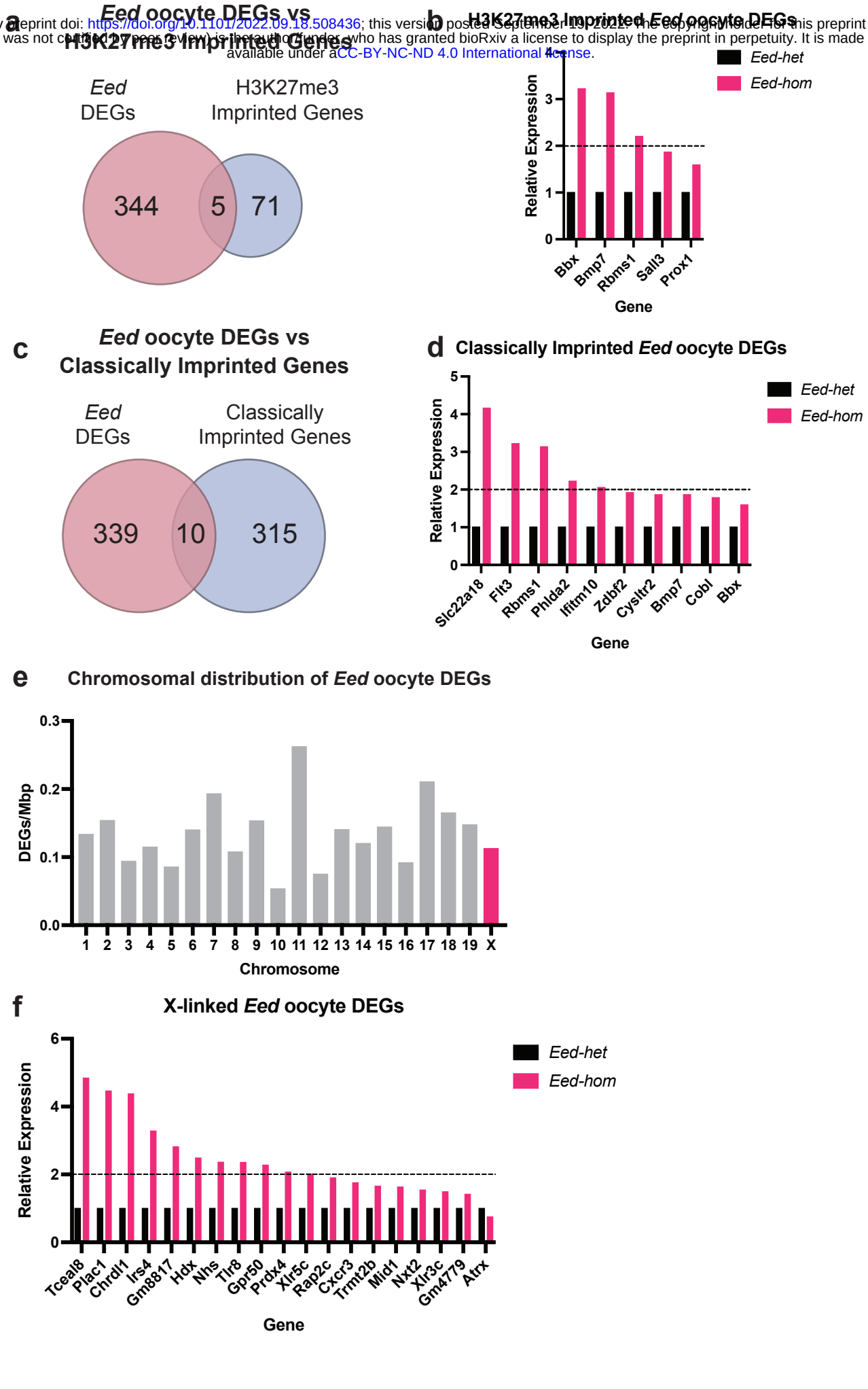

Fig 5

887 **Fig 5. EED is required for repressing a wide range of genes in growing oocytes that are not**
888 **canonically or non-canonically imprinted or X-linked genes (a)** Venn diagram comparing *Eed*
889 oocyte DEGs against putative H3K27me3 imprinted genes (35). **(b)** Expression of putative
890 H3K27me3 imprinted *Eed* oocyte DEGs in *Eed-hom* oocyte relative to *Eed-het*. Data represent the
891 mean transcripts per million (TPM), with *Eed-het* mean set to 1.0. **(c)** Venn diagram comparing
892 *Eed* oocyte DEGs against known or predicted classically imprinted genes (49, 50). **(d)** Expression
893 of known or predicted classically imprinted *Eed* oocyte DEGs in *Eed-hom* oocyte relative to *Eed-*
894 *het*. Data represent the mean transcripts per million (TPM), with *Eed-het* mean set to 1.0. **(e)**
895 graphical representation of *Eed* oocyte DEGs per mega base vs chromosome for autosome and
896 the X-chromosome. **(f)** Expression of X-linked *Eed* oocyte DEGs in *Eed-hom* oocyte relative to *Eed-*
897 *het*. Data represent the mean transcripts per million (TPM), with *Eed-het* mean set to 1.0.
898
899

a

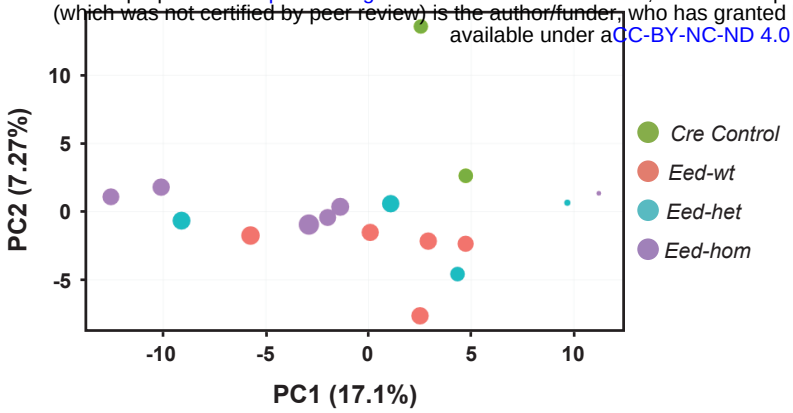

b

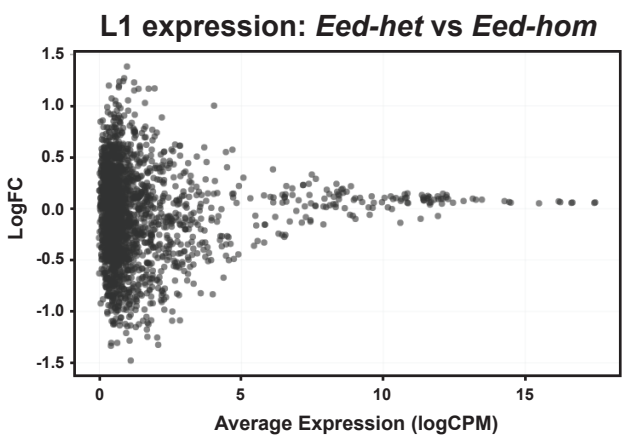

Fig 6

Fig 6. Loss of *Eed* in growing oocytes did not impact expression of LINE-1 transposons. (a) Principal Component Analysis (PCA) of RNA-seq data for L1 elements in *Eed-hom* (n=6) vs *Eed-het* (n=4), *Eed-wt* (n=5) and *Eed-wt Cre* (n=2) controls. **(b)** Differential expression analysis of L1 elements for *Eed-het* versus *Eed-hom* females.

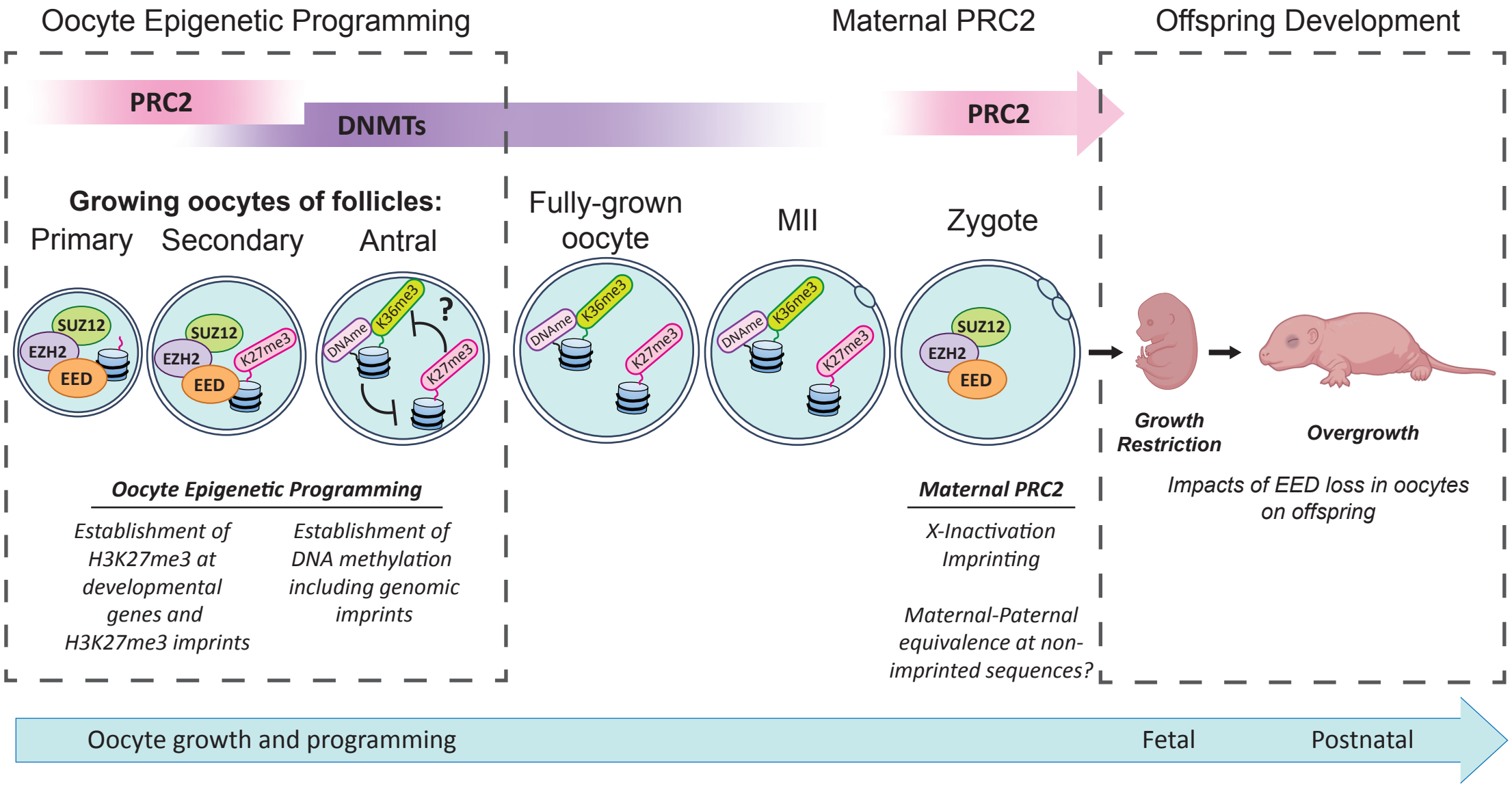
Oocyte Epigenetic Programming
Maternal PRC2
Offspring Development
PRC2
DNMTs
PRC2
Growing oocytes of follicles:
Primary
Secondary
Antral
Fully-grown oocyte
MII
Zygote
SUZ12
EZH2
EED
K27me3
DNAme
K36me3
?
Growth Restriction
Overgrowth
Oocyte Epigenetic Programming
Establishment of H3K27me3 at developmental genes and H3K27me3 imprints
Establishment of DNA methylation including genomic imprints
Maternal PRC2
X-Inactivation
Imprinting
Maternal-Paternal equivalence at non-imprinted sequences?
Impacts of EED loss in oocytes on offspring
Oocyte growth and programming
Fetal
Postnatal

Fig 7

908 **Fig 7: Summary of PRC2 functions during oocyte growth and maturation and pre-implantation**
909 **development.** All three essential components of PRC2 are present in growing oocytes only at the
910 primary to secondary stages and establish H3K27me3 on H3K27me3 imprinted genes and a wide
911 range of developmental genes, potentially programming *Eed* oocyte DEG expression in offspring.
912 As this activity immediately precedes *de novo* DNA methylation, we propose that H3K27me3
913 established prior to DNA methylation may act as a "place-keeper" protecting developmental
914 genes from modifications such as H3K36me3 and/or DNA methylation. Cytoplasmic PRC2
915 proteins and/or mRNA are inherited via the mature oocyte and regulate pre-implantation
916 development, including X-inactivation, H3K27me3 dependent imprinting (31, 34, 35) and
917 establishment of maternal – paternal equivalence at non-imprinted sequences. Loss of PRC2 in
918 the oocyte leads to embryo growth restriction (33) but offspring are ultimately overgrown
919 immediately after birth (40).
920